




# Effect of Calcination on Morphology of Zinc Oxide Nanoparticles

Subodh Kumar<sup>a</sup>, Ram Pal Tandon<sup>a</sup>, and Ajit K. Mahapatro<sup>a,b</sup> 

<sup>a</sup>Department of Physics & Astrophysics, University of Delhi, New Delhi, India; <sup>b</sup>Department of Physics & Astronomy, University of the Western Cape, Bellville, Cape Town, South Africa

## ABSTRACT

Zinc oxide (ZnO) nanoparticles are synthesized using the sol-gel method by considering zinc acetate dihydrate as a precursor, and the morphology and crystalline structure of the as-synthesized ZnO nanoparticles are understood using materials characterization techniques. The effect of calcination temperature and time on the morphology of ZnO powder is studied thoroughly and systematically. The recipe for preparing highly pure ZnO powders is optimized at minimal calcination temperature and time. The powder X-ray diffraction analysis reveals a wurtzite crystal structure for ZnO nanoparticles (ZnO-NPs). From the diffraction patterns, it is evident that the powders calcined at 700 °C for 3 h closely match the JCPDS standard for minimal calcination temperature and time. The peak at 364.48 cm<sup>-1</sup> in the Fourier transform infrared spectroscopy provides information about the bonding interaction between Zn and O in ZnO-NPs. The UV-Visible absorption spectra of ZnO-NPs indicate a shifting of peak from 374.37 to 378.49 nm, and the corresponding Tauc plot estimates a change in band gap from 2.461 eV to 2.847 eV for ZnO prepared with calcined at 700 °C for 3 h and 6 h, respectively, due to change in morphology and particle size. The field emission scanning electron microscopy (FESEM) images indicate the formation of spherical-shaped nanoparticles with smooth surfaces and EDAX spectra reveal compositions of zinc and oxygen-only ZnO-NPs. Noticeable changes in the particle size and morphology are observed with increasing calcination temperature. The Raman spectra of the ZnO-NPs recorded using a 514 nm excitation wavelength indicate E2(high) mode at 437.5 cm<sup>-1</sup> in ZnO-NPs prepared by calcining at 700 °C for 3 h. The optimal condition for achieving high pure ZnO-NPs with well-defined morphology is concluded by calcining the ZnO powder at 700 °C for a duration of 3 h.

## KEYWORDS

Zinc oxide nanoparticles; sol-gel; crystalline structure; FESEM and EDAX

## 1. Introduction

Zinc oxide (ZnO) is a versatile semiconducting material with a wide range of applications in electronic, optoelectronic, and photonic devices [1]. Sol-gel method is a well-established technique for the synthesis of nano-structure materials, which offers a low-cost, simple, and scalable route for the production of high-quality materials with

controlled size and morphology [1,2]. The sol-gel process involves the formation of a colloidal solution, or sol, by hydrolysis and condensation of metal alkoxides or salt in a liquid medium. In this method, a metal alkoxide precursor, usually zinc acetate or zinc nitrate, is hydrolyzed to form a metal oxide gel. The gel is heated to remove the solvent and organic components, leaving behind a porous metal oxide powder. The particle size and morphology of the ZnO nanoparticles (ZnO-NPs) can be controlled by adjusting the concentration of the precursor, the pH of the solution, calcination temperature, and time [3,4]. The sol-gel synthesis of ZnO-NPs offers several advantages over other methods, such as chemical vapor deposition (CVD) and physical vapor deposition (PVD) [4]. Sol-gel method allows the production of nanoparticles and nanorods with high purity and uniform size distribution, as well as the incorporation of dopants and the formation of complex nanostructure [5,6].

This study aims to synthesize ZnO-NPs by sol-gel method, The objective of this study is to employ a cost-effective sol-gel method for synthesizing ZnO-NPs at minimal calcination temperature and time and to explore their structural and morphological characteristics. The as-synthesized nanoparticles are characterized by various techniques, such as X-ray diffraction (XRD), field emission scanning electron microscopy (FESEM), energy dispersive X-ray (EDAX) analysis, UV-Vis spectroscopy, Fourier transform infrared spectroscopy (FTIR), and Raman spectroscopy to find an optimized recipe for preparing highly pure ZnO-NPs. The temperature and duration of the calcination process affect the size and morphology of the as-synthesized ZnO-NPs. The XRD, Raman, FESEM, and EDAX are performed on the as-synthesized ZnO-NPs calcined at 600 °C, 700 °C, 800 °C, 900 °C, and 1000 °C for 3 h and 6 h. The highly pure hexagonal wurtzite structure of ZnO-NPs with well-defined morphology is achieved in the recipe followed by calcining the ZnO powder at 700 °C for a duration of 3 h.

## **2. Experimental section**

### **2.1. Materials**

The precursors zinc acetate dihydrate (99.5% pure), alcohol (99.9% pure), and hydrogen peroxide (30% w/v), and all other chemicals used in this experiment are procured from Thermo Fisher Scientific, USA.

### **2.2. Synthesis of zinc oxide nanoparticles (ZnO-NPs)**

The sol-gel method was adopted to produce ZnO-NPs, initiated by dissolving 12.6 g of zinc acetate dihydrate ( $\text{Zn}(\text{CH}_3\text{COO})_2 \cdot 2\text{H}_2\text{O}$ ) in 400 ml of double distilled water with continuous stirring. The solution was heated to 50 °C and 600 ml of ethanol was added by maintaining the stirring process. Then, 6 ml of hydrogen peroxide ( $\text{H}_2\text{O}_2$ ) (30% w/v) was added dropwise and mixed using a magnetic stirrer until the realization of a homogeneous solution. The resulting solution was then incubated for 24 h and heated at 80 °C for several hours till the formation of the white-colored solution containing zinc oxide nanoparticles. The resulting solution was centrifuged for 10 min and the precipitate was separated out. The ZnO nanoparticles were then washed three times with deionized water and several times with ethanol to remove any byproducts that were

bound to the nanoparticles. The nanoparticles were dried in an open-air hot plate at approximately 80 °C till production of white powder form followed by calcination at 600 °C, 700 °C, 800 °C, 900 °C, and 1000 °C for 3 h (S236, S237, S238, S239 and S2310) and 6 h (S266, S267, S268, S269 and S2610), respectively.

### 2.3. Characterization techniques

X-ray Diffraction (XRD) patterns of ZnO-NPs were recorded using a Malvern Panalytical Empyrean Diffractometer. The diffractometer was operated at 45 kV and 40 mA current, with Cu-K $\alpha$  ( $\lambda = 1.54 \text{ \AA}$ ) radiations serving as the source of X-rays. The instrument recorded the spectrum in the  $2\theta$  range of  $20^\circ$  to  $80^\circ$  using a slow scan speed and a slow scan rate of  $2^\circ/\text{min}$ . Fourier Transform Infrared Spectroscopy (FTIR) spectra of all the samples, were obtained using the ATR-FTIR mode of a Thermo Fisher Scientific (Model-Nicolet IS50, USA) spectrophotometer. The spectrophotometer has a range of  $400 \text{ cm}^{-1}$  to  $4000 \text{ cm}^{-1}$  and a resolution of  $1 \text{ cm}^{-1}$ . UV-visible spectroscopy (UV-VIS) spectroscopy of ZnO-NPs was conducted using a Perkin Elmer (Lambda-950, USA) double-beam dual monochromator spectrometer. The spectrometer has a wavelength range extending from 3300 to 175 nm. A photomultiplier type R6872 is used as a detector for the UV-VIS range. The ZnO-NPs were subjected to Raman spectroscopy examination using a Renishaw (model-inVia RE02) that used a 150 W power laser with a wavelength of 514 nm. The morphology of ZnO nanoparticles was analyzed using a ZEISS Gemini-500 field emission scanning electron microscope. The nanoparticles were coated with gold and viewed under the FESEM with different magnifications and an accelerating voltage of 15.0 kV. The elemental composition is analyzed using the EDAX Elect Super system with a  $70 \text{ mm}^2$  sensor size.

## 3. Results and discussions

### 3.1. X-ray diffraction (XRD) analysis

The crystal structure of ZnO-NPs is analyzed using XRD. The diffraction from various planes of ZnO-NPs shows peaks recorded at  $2\theta$  values and their corresponding hkl plane of  $31.72^\circ$  (100),  $34.40^\circ$  (002),  $36.21^\circ$  (101),  $47.49^\circ$  (102),  $56.52^\circ$  (110),  $62.80^\circ$  (103),  $66.28^\circ$  (200),  $67.86^\circ$  (112),  $68.99^\circ$  (201),  $72.5^\circ$  (004) and  $76.86^\circ$  (202) correspond to the hexagonal wurtzite structure, as indexed in the JCPDS card no. 036- 1451 (Figure 1a and b). The XRD pattern shows intense peaks of (100) and (101) planes, which increase with an increase in calcination temperature. The average crystallite size and lattice parameters (a, b, and c) of the ZnO-NPs were determined from the analysis of diffraction peak positions and intensities. The calculated lattice parameters for ZnO-NPs a = b, and c is approximately  $3.24 \text{ \AA}$  and  $5.19 \text{ \AA}$ , respectively, resulting in a c/a ratio of 5.19. The average crystallite size was assessed for ZnO-NPs subjected to calcination at temperatures of 600 °C, 700 °C, 800 °C, 900 °C, and 1000 °C for both 3 h and 6 h durations. These samples were designated as S236, S237, S238, S239, S2310 (for 3 h), and S266, S267, S268, S269, and S2610 (for 6 h). The Debye-Scherrer formula ( $D = k\lambda/\beta\cos\theta$ ) is used for the determination of average crystal size, where,  $k = 0.98$  is the Scherrer constant,  $\lambda = 1.54 \text{ \AA}$  is the excitation wavelength,  $\beta$  is the full width at half

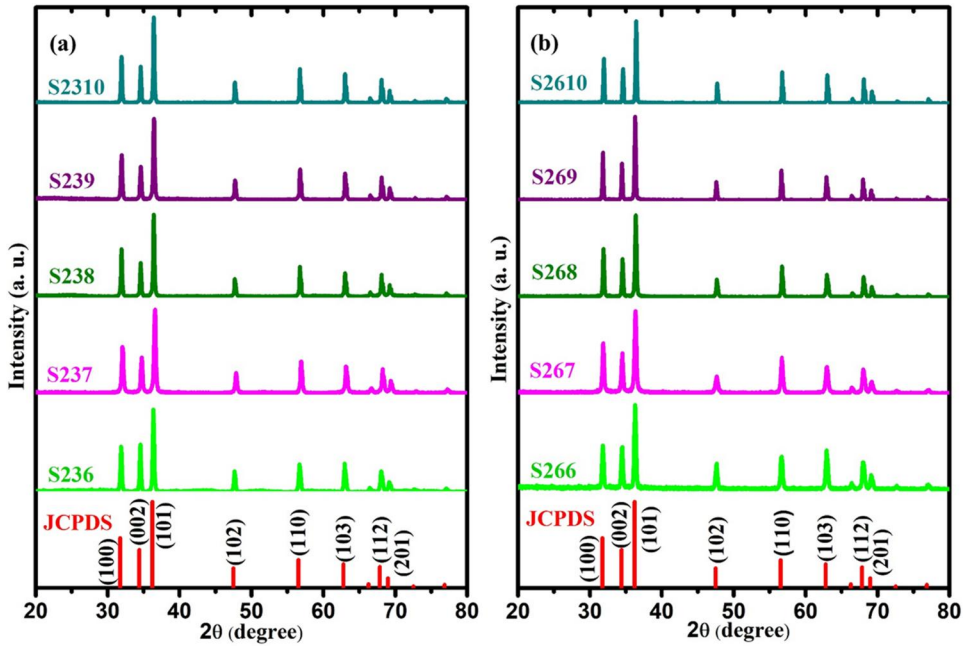


**Figure 1.** The XRD Spectra of ZnO-NPs samples calcined for (a) 3 h at temperatures of 600 °C, 700 °C, 800 °C, 900 °C and 1000 °C. and (b) 6 h at temperatures of 600 °C, 700 °C, 800 °C, 900 °C and 1000 °C.

**Table 1.** ZnO powder calcined for 3 h at temperatures of 600 °C, 700 °C, 800 °C, 900 °C, and 1000 °C.

Sample	a = b (Å)	c (Å)	Ratio c/a	% Error in a	% error in c	Avg. crystallite size (nm)	Lattice strain
S236	3.246	5.192	1.599	0.08	0.27	31.3	0.003
S237	3.238	5.162	1.594	0.32	0.84	29.12	0.004
S238	3.245	5.188	1.598	0.13	0.34	35.9	0.003
S239	3.245	5.184	1.597	0.16	0.42	34.71	0.003
S2310	3.245	5.184	1.597	0.16	0.42	38.36	0.003

**Table 2.** ZnO powder calcined for 6 h at temperatures of 600 °C, 700 °C, 800 °C, 900 °C, and 1000 °C.

Sample	a = b (Å)	c (Å)	Ratio c/a	% Error in a	% Error in c	Avg. Crystallite size (nm)	Lattice strain
S266	3.247	5.212	1.605	0.07	0.12	27.41	0.004
S267	3.247	5.194	1.599	0.07	0.23	25.87	0.004
S268	3.247	5.194	1.599	0.07	0.23	33.72	0.003
S269	3.247	5.194	1.599	0.07	0.23	39.26	0.003
S2610	3.247	5.172	1.593	0.07	0.65	40.69	0.003

maximum of the diffraction peak, and  $2\theta$  is the angle between the incident and diffracted beams. The average crystallite size ranged from 29.12 nm to 38.36 nm for the 3-hour calcination and from 25.87 nm to 40.69 nm for the 6-hour calcination, as the temperature increased from 600 °C to 1000 °C. These values are tabulated in [Table 1](#) and [Table 2](#). [Figure 2a](#) and [b](#) depict the increase in average crystallite size as the calcination temperature rises for both the 3-hour and 6-hour processes. This indicates an increase in calcination temperature promotes processes that favor the growth of crystallites, resulting in an increase in crystallite size. The XRD patterns suggest that achieving pure ZnO-NPs without impurities requires a minimum calcination time of 3 h and a

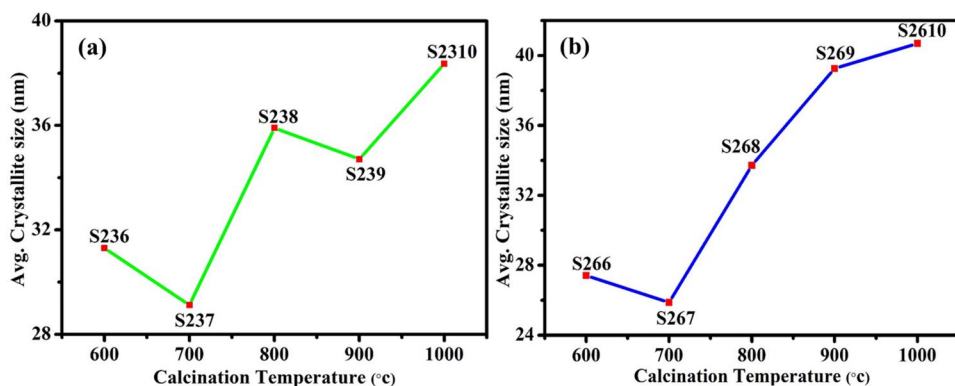


**Figure 2.** Average crystallite size of ZnO-NPs calcined for (a) 3 h at temperatures of 600 °C, 700 °C, 800 °C, 900 °C and 1000 °C. (b) 6 h at temperatures of 600 °C, 700 °C, 800 °C, 900 °C and 1000 °C.

temperature of 700 °C. Among all the calcined powders, the S237 powder exhibits the lowest temperature and time requirement. Consequently, it has been selected as the optimized sample for further investigation of materials characterization.

### 3.2. FTIR analysis

The FT-IR spectra of ZnO-NPs are shown in Figure 3. The S2 and S236 samples show various peaks at 2160.24  $\text{cm}^{-1}$ , 1537.27  $\text{cm}^{-1}$ , 1400.37  $\text{cm}^{-1}$ , 985.24  $\text{cm}^{-1}$ , 864.97  $\text{cm}^{-1}$ , 686.49  $\text{cm}^{-1}$  and 570.12  $\text{cm}^{-1}$ . The peak at 2160.24  $\text{cm}^{-1}$  is observed due to  $\text{CO}_2$  molecules in air, and the bond at 985.24  $\text{cm}^{-1}$  is due to C-O stretching vibration [7,8]. The peaks at 1537.27  $\text{cm}^{-1}$  and 1400.37  $\text{cm}^{-1}$  are corresponding to the asymmetric and symmetric stretching of the carboxyl group, respectively. Peaks in the range of 864.97  $\text{cm}^{-1}$  to 570.12  $\text{cm}^{-1}$  indicate the metal-oxygen (Zn-O stretching vibration) vibration mode [7–11]. ZnO-NPs in samples S2 and S236 exhibited multiple distinct functional groups associated with ZnO. As the calcination temperature increased, these functional groups were progressively eliminated. In the case of S237, S238, S239, and S2310, only a single peak at 420.2  $\text{cm}^{-1}$  remained, corresponding to the Zn-O stretching vibration [12]. This observation suggests that ZnO nanoparticles in sample S237 reached the minimal time and temperature requirements to achieve a state of purity and support the XRD analysis.

### 3.3. Raman spectroscopy

Figure 4 shows the Raman spectra of ZnO-NPs prepared as S236, S237, S238, S239, and S2310. The notable peak observed at 437.5  $\text{cm}^{-1}$  is indicative of the Raman activity in all ZnO-NPs. This peak corresponds to the E2(high) phonon mode of ZnO-NPs [13]. The E2(high) mode is associated with the vibration of oxygen atoms within the crystal lattice along the c-axis of the wurtzite crystal structure of ZnO [13–15], and this well-recognized characteristic Raman peak is frequently used for identifying the presence of ZnO in a sample [13].

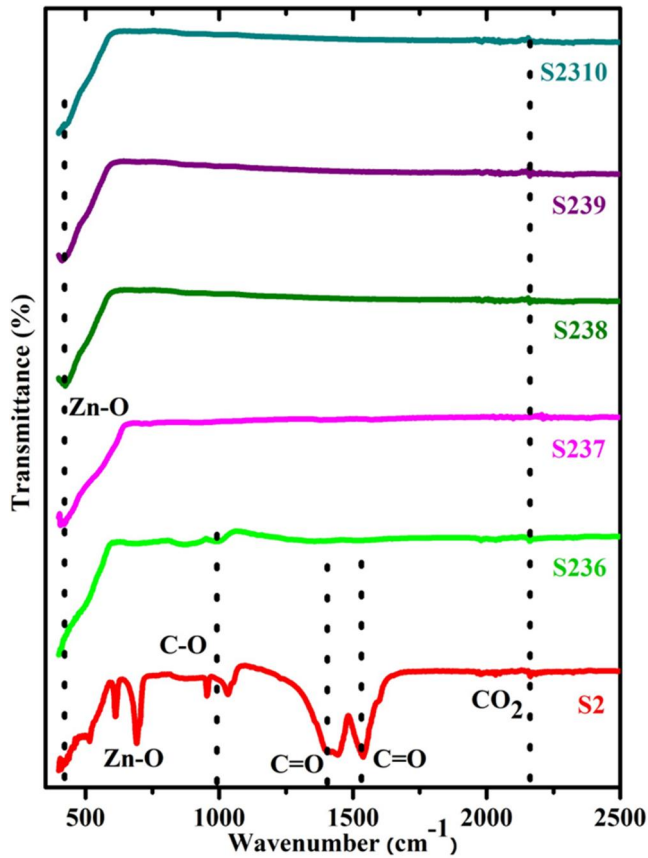


**Figure 3.** FTIR spectrum of ZnO-NPs for as-synthesis ZnO-NPs without calcination (S2), and after calcination at 600 °C, 700 °C, 800 °C, 900 °C and 1000 °C, for 3 h.

### 3.4. FESEM

The morphology of ZnO-NPs prepared as S236, S237, S266, and S267, is through FESEM imaging and depicted in Figures 5a, b, 6a, b, 7a, b, 8a, and b. These images reveal ZnO nanoparticles characterized by well-defined surfaces with structures resembling pebbles. An increase in calcination temperature from 600 °C (S236) to 700 °C (S237) for 3 h results in a particle size enlargement from  $83 \pm 2.45$  nm to  $120 \pm 1.88$  nm. Similarly, with a rise in calcination temperature from 600 °C (S266) to 700 °C (S267) for 6 h, the particle size increases from  $1.259 \pm 0.04$   $\mu\text{m}$  to  $1.811 \pm 0.06$   $\mu\text{m}$ . The particle size distribution for ZnO-NPs S236, S237, S266, and S267 is presented in Figures 5c, 6c, 7c, and 8c, respectively.

The elemental compositions are identified through EDAX measurements, as depicted in Figures 5d, 6d, 7d, and 8d. These images show that ZnO-NPs consist of only zinc and oxygen, which indicates the purity of the samples. The above observations suggest that all the particles exhibit a near-spherical shape, and as the calcination time increases ZnO-NPs undergo morphological changes with distinct and well-separated grain boundaries [9,16,17].

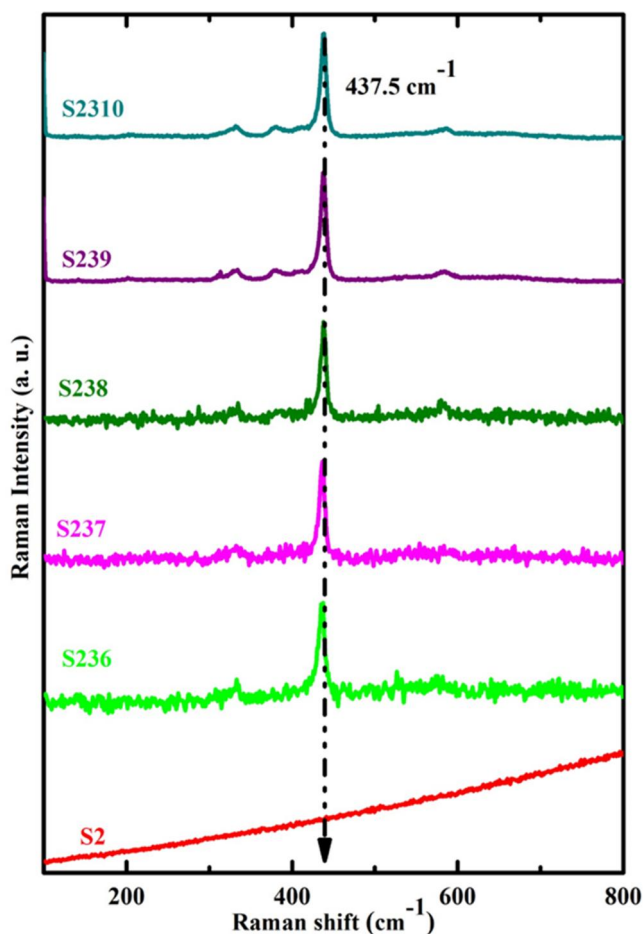


**Figure 4.** Raman spectroscopy of as-synthesis ZnO nanoparticles without calcination (S2), and after calcination at 600 °C, 700 °C, 800 °C, 900 °C and 1000 °C, for 3 h.

### 3.5. UV-Visible spectroscopy

The optical characteristics of the ZnO-NPs were explored through UV-visible spectroscopy. The UV-visible absorbance spectrum of the ZnO-NPs recorded by dispersing in ethanol is presented in Figures 9a and b. Notably, the absorption peak centered at 374.37 and 378.49 nm, represents the distinctive hallmark of hexagonal wurtzite ZnO [5,7]. The absorbance peak observed at 374.37 nm for S237 corresponds to the bandgap absorption of the material. When the calcination time is extended to 6 h for S267, the peak undergoes a shift to 378.49 nm. This shift can be attributed to changes in the particle size and morphology of the ZnO-NPs, as revealed by the FESEM study [7]. The calculated band gap for S237 is found to be 2.461 eV and for S267 is 2.847 eV [18,19], as illustrated in the Tauc plots that involve plotting graphs with  $(\alpha h\nu)^2$  versus  $h\nu$  and extrapolating the linear segment in Figure 10a and b, respectively. These findings indicate that the ZnO-NPs are capable of absorbing UV light with a wavelength shorter than approximately 370 nm. The bandgap absorption arises for ZnO-NPs is from the

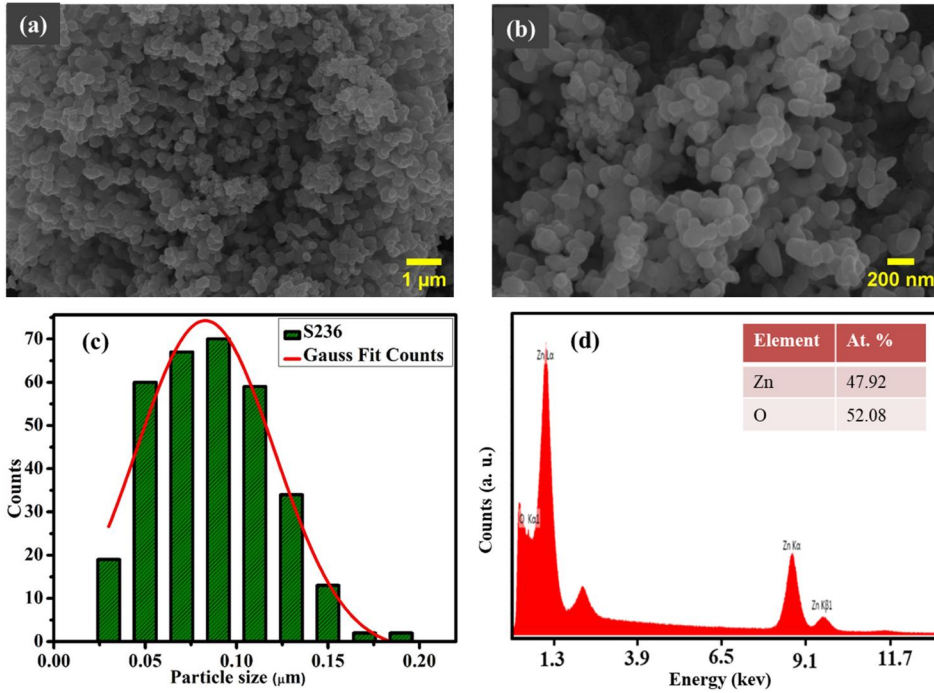


**Figure 5.** S2 Sample calcined at 600 °C for 3 h (S236) (a, b) FESEM images of S236 (c) Particle size distribution of S236 (d) EDAX spectra of S236.

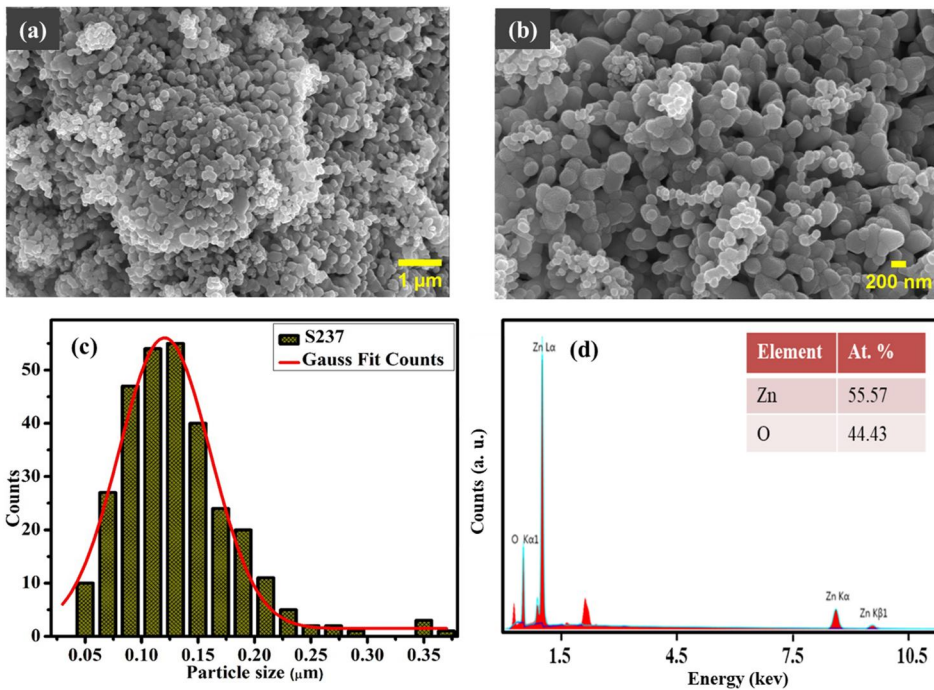


**Figure 6.** S2 Sample calcined at 700 °C for 3 h (S237) (a, b) FESEM images of S237 (c) Particle size distribution of S237 (d) EDAX spectra of S237.

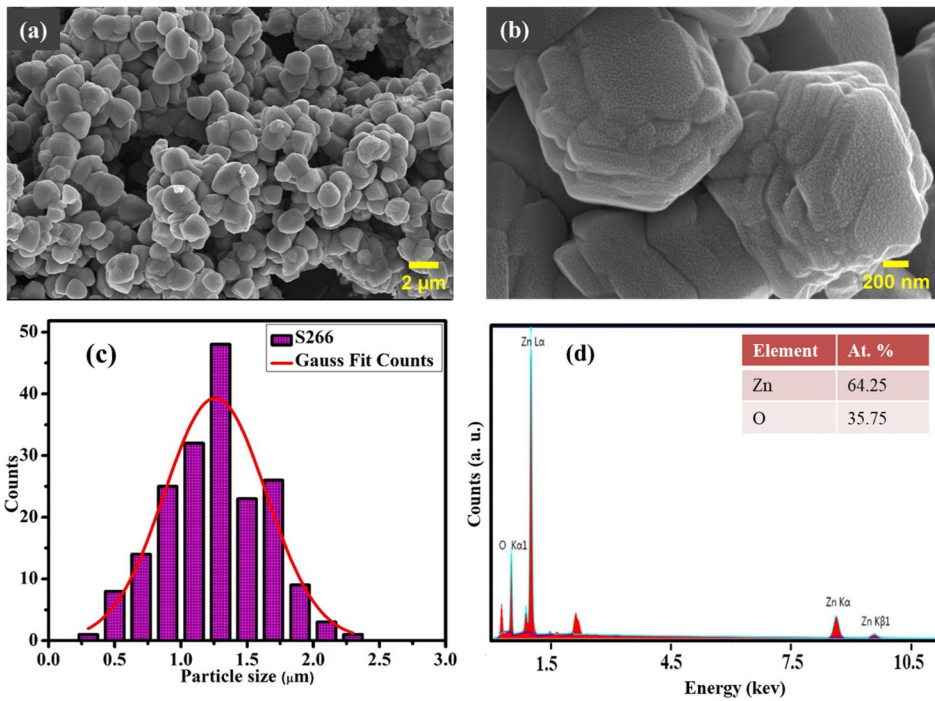


**Figure 7.** S2 Sample calcined at 600 °C for 6 h (S266) (a, b) FESEM images of S266 (c) Particle size distribution of S266 (d) EDAX spectra of S266.

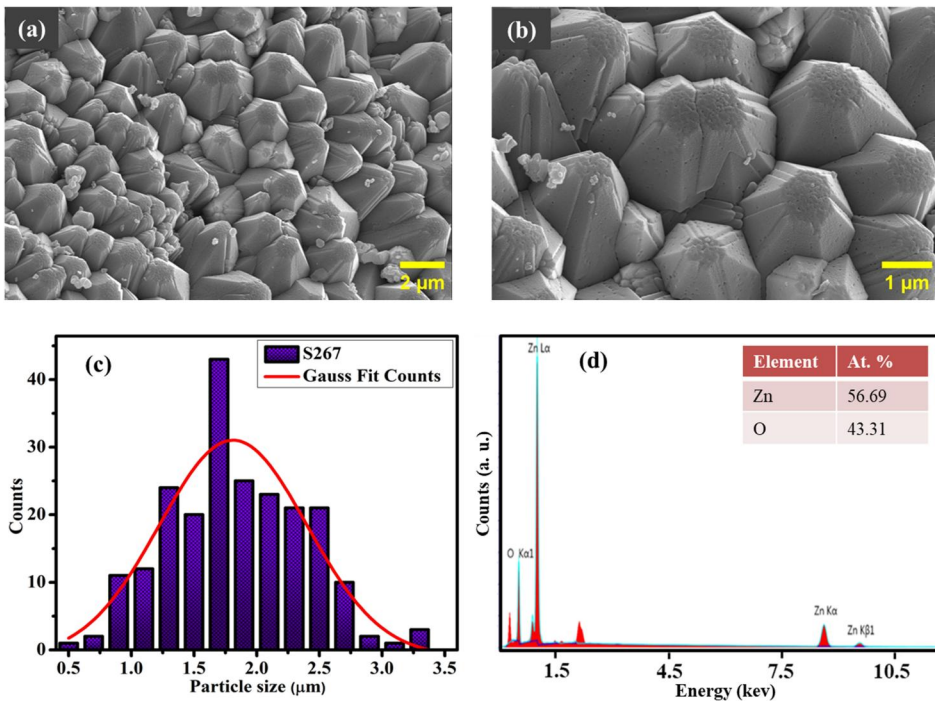


**Figure 8.** S2 Sample calcined at 700 °C for 6 h (S267) (a, b) FESEM images of S267 (c) Particle size distribution of S267 (d) EDAX spectra of S267.

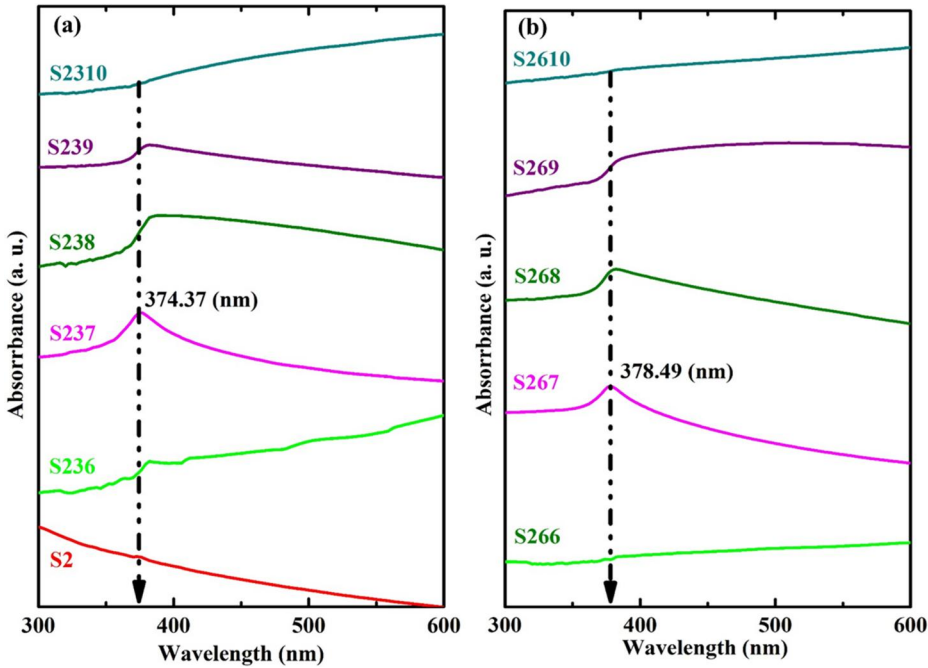


**Figure 9.** The UV-Vis optical absorption spectrum of ZnO-NPs calcined at temperatures of 600 °C, 700 °C, 800 °C, 900 °C and 1000 °C. for (a) 3 h and (b) 6 h.

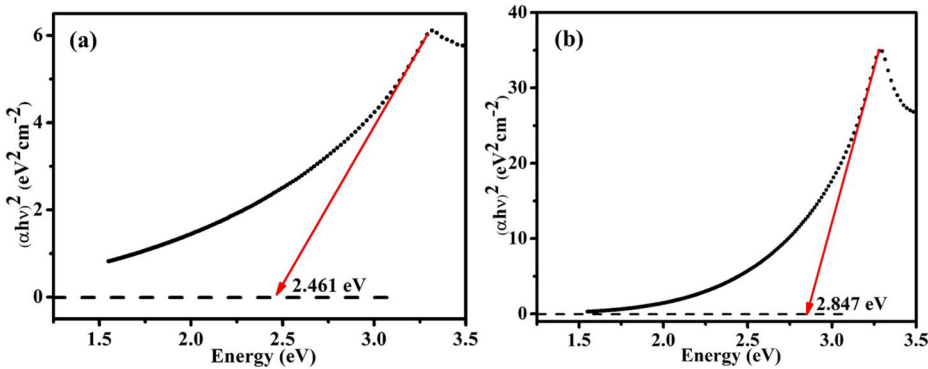


**Figure 10.** Tauc plot of  $(\alpha h\nu)^2$  versus  $h\nu$  for the sample (a) S237 and (b) S267.

transition of electrons from the valence band to the conduction band, and contributes to the electrical and optical properties [5,7,8,11,17].

#### 4. Conclusion

This study describes the synthesis of highly pure zinc oxide (ZnO) nanoparticles using a straightforward and cost-effective sol-gel method. The as-synthesized ZnO nanoparticles exhibit a spherical shape with a hexagonal wurtzite structure. The XRD patterns reveal intense peaks associated with the (100) and (101) crystallographic planes, which become

more prominent as the calcination temperature increases. The results suggest that achieving pure ZnO nanoparticles without impurities requires a specific minimum calcination time and temperature, with sample S237 demonstrating the lowest temperature and time requirements. The average crystallite size increases with higher calcination temperature and time. FESEM images illustrate spherical-shaped nanoparticles with well-separated grain boundaries. EDAX analysis confirms the purity of the synthesized ZnO nanoparticles, consisting only of zinc and oxygen elements. The UV-visible absorbance peaks at 374.37 nm for sample S237 (calcined at 700 °C for 3 h) and 378.49 nm for sample S267 (calcined at 700 °C for 6 h) correspond to bandgap absorption, indicating changes in particle size and morphology, as supported by FESEM. Raman spectroscopy of ZnO shows the characteristic E2(high) mode peak at 437.5 cm<sup>-1</sup>. The high yield and scalability of the synthesis method make it well-suited for large-scale production of ZnO nanoparticles. These highly pure ZnO-NPs hold potential for future applications in electronic and thermoelectric devices, as well as photocatalysis, gas sensing, biomedical devices, and solar protection products.

## Acknowledgements

The authors would thank the Central Experimental Facilities (CEF) at the Department of Physics & Astrophysics and USIC, University of Delhi, New Delhi-110007, for providing the necessary resources and facilities to carry out this research. The authors acknowledge the financial assistance provided by IoE (ref. No./IoE/2022-23/FRP/and ref. No./IoE/2023-24/12/FRP) through the FRP scheme. SK thanks the University Grant Commission (UGC - NFSC) for providing a fellowship to pursue Ph.D. program.

## Disclosure statement

No potential conflict of interest was reported by the author(s).

## ORCID

Ajit K. Mahapatro  <http://orcid.org/0000-0002-3860-2862>

## References

1. C. Klingshirn, ZnO: Material, physics and application, *Chemphyschem* **8** (6), 782 (2007). DOI: [10.1002/cphc.200700002](https://doi.org/10.1002/cphc.200700002).
2. D. Bokov *et al.*, Nanomaterial by Sol-Gel method: Synthesis and application, *Advances in Mater. Sci. Eng.* **2021** (1), 5102014 (2021). DOI: [10.1155/2021/5102014](https://doi.org/10.1155/2021/5102014).
3. T. Jin *et al.*, Antimicrobial efficacy of zinc oxide quantum dots against *Listeria monocytogenes*, salmonella enteritidis and *Escherichia coli*, 0157: H7, *J. Food Sci.* **74** (1), M46 (2009). DOI: [10.1111/j.1750-3841.2008.01013.x](https://doi.org/10.1111/j.1750-3841.2008.01013.x).
4. J. N. Hasnidawani *et al.*, Synthesis of ZnO nanostructures using sol-gel method, *Procedia Chem.* **19**, 211 (2016). DOI: [10.1016/j.proche.2016.03.095](https://doi.org/10.1016/j.proche.2016.03.095).
5. H. Morkoç, and Ü. Özgür, 2009 Chapter 1 general properties of ZnO. In *Zinc Oxide: Fundamentals. Materials and Device Technology*, Wiley-VCH.
6. R. M. Alwan *et al.*, Synthesis of zinc oxide nanoparticles via sol – gel route and their characterization, *Nanosci. Nanotechnol.* **5** (1), 1 (2015).

7. R. N. Mariammal *et al.*, Role of heterojunction and oxygen vacancies on ethanol detection by ZnO:SnO<sub>2</sub> nanocomposites, *Adv. Sci. Lett.* **17** (1), 56 (2012). DOI: [10.1166/asl.2012.4259](https://doi.org/10.1166/asl.2012.4259).
8. N. Jayarambabu *et al.*, Germination and growth characteristics of mungbean seeds (*Vigna radiata* L.) affected by synthesized zinc oxide nanoparticles, *Int. J. Current Eng. Technol.* **4** (5) (2014).
9. S. Jurablu, M. Farahmandjou, and T. P. Firoozabadi, Sol-gel synthesis of zinc oxide (ZnO) nanoparticles: study of structural and optical properties, *J. Sci. Islamic Repub. Iran* **26** (3), 281 (2015).
10. J. Coates, *Interpretation of Infrared Spectra, A Practical Approach*, John Wiley & Sons Ltd, Chichester, 2000
11. N. Jayarambabu, and B. Siva Kumari, Beneficial Role of Zinc Oxide Nanoparticles on Green Crop Production. *Int. J. Multidisciplinary Adv. Res. Trends* **II** (I), 2349 (2015).
12. A. R. Abhijith, A. K. Srivastava, and A. Srivastava, Synthesis and characterization of magnesium doped ZnO using chemical route, *J. Phys: Conf. Ser.* **1531** (1), 12005 (2020). DOI: [10.1088/1742-6596/1531/1/012005](https://doi.org/10.1088/1742-6596/1531/1/012005).
13. A. Khan, W. M. Jadwisieniczak, and M. E. Kordesch, *Materials Research Society* **900**, 158 (2005).
14. T. C. Damen, S. P. S. Porto, and B. Tell, *Raman Effect in Zinc Oxide* **142** (2) (1966).
15. M. Šćepanović *et al.*, Raman study of structural disorder in ZnO nanopowder, *J. Raman Spectroscopy* **41** (9), 914 (2010). DOI: [10.1002/jrs.2546](https://doi.org/10.1002/jrs.2546).
16. A. A. Al-Owais, Synthesis and magnetic properties of hexagonally packed ZnO nanorods, *Arabian J. Chem.* **6** (2), 229 (2013). DOI: [10.1016/j.arabjc.2011.11.001](https://doi.org/10.1016/j.arabjc.2011.11.001).
17. M. Pudukudy, and Z. Yaakob, Facile synthesis of quasi spherical ZnO nanoparticles with excellent photocatalytic activity, *J. Cluster Sci.* (2014).
18. L. T. Jule *et al.*, Wide visible emission and narrowing band gap in Cd-doped ZnO nanopowders synthesized via sol-gel route, *J. Alloys Compd.* **687**, 920e (2016). DOI: [10.1016/j.jallcom.2016.06.176](https://doi.org/10.1016/j.jallcom.2016.06.176).
19. A. S. Shahvelayati, M. Sabbaghan, and S. E. Bashtani, Imidazolium-based ionic liquids on morphology and optical properties of ZnO nanostructures, *Int. J. Nanosci. Nanotechnol.* **11** (2), 123 (2015).
20. N. Sangeetha, and L. Kumaragura, Extracellular synthesis of zinc oxide nanoparticles using seaweeds of Gulf of Manar, Indani. *J. Nanobiotechnol.* **11** (39), 1 (2013).
21. P. Fageria, S. Gangopadhyay, and S. Pande, Synthesis of ZnO/Au and ZnO/Ag nanoparticles and their photocatalytic application using UV and visible light, *RSC Adv* **4** (48), 24962 (2014). DOI: [10.1039/C4RA03158J](https://doi.org/10.1039/C4RA03158J).
22. I. Radyum, R. I. Putri, and S. Siswanto, Effect of PH variation on particle size and purity of Nano zinc oxide synthesized by sol-gel method, *Int. J. Eng. Technol.* **12** (6), 5 (2012).